

Two-step dimensionality reduction of human mobility data: From potential landscapes to spatiotemporal insights

Yunhan Du¹, Takaaki Aoki², Naoya Fujiwara^{1,3,4,5*}

¹Graduate School of Information Sciences, Tohoku University, 6-3-09
Aoba, Aramaki, Aoba, Sendai, 980-8579, Miyagi, Japan.

²Graduate School of Data Science, Shiga University, 1-1-1, Banba,
Hikone, 522-8522, Shiga, Japan.

³PRESTO, Japan Science and Technology Agency, 4-1-8 Honcho,
Kawaguchi, 332-0012, Saitama, Japan.

⁴Center for Spatial Information Science, The University of Tokyo, 5-1-5
Kashiwanoha, Kashiwa, 277-8568, Chiba, Japan.

⁵Institute of Industrial Science, The University of Tokyo, 4-6-1 Komaba,
Meguro-ku, 153-8505, Tokyo, Japan.

*Corresponding author(s). E-mail(s): naoya.fujiwara@tohoku.ac.jp;

Contributing authors: du.yunhan.q8@dc.tohoku.ac.jp;
takaaki-aoki@biwako.shiga-u.ac.jp;

Abstract

Understanding the spatiotemporal patterns of human mobility is crucial for addressing societal challenges, such as epidemic control and urban transportation optimization. Despite advancements in data collection, the complexity and scale of mobility data continue to pose significant analytical challenges. Existing methods often result in losing location-specific details and fail to fully capture the intricacies of human movement. This study proposes a two-step dimensionality reduction framework to overcome existing limitations. First, we construct a potential landscape of human flow from origin-destination (OD) matrices using combinatorial Hodge theory, preserving essential spatial and structural information while enabling an intuitive visualization of flow patterns. Second, we apply

⁰Google scholar profiles: Yunhan Du <https://scholar.google.com/citations?user=zgv6kzkAAAAJ&hl=en>; Takaaki Aoki <https://scholar.google.com/citations?user=e8x3baAAAAAJ&hl=en>; Naoya Fujiwara <https://scholar.google.co.jp/citations?user=qmt1jPMAAAAJ&hl=en>

principal component analysis (PCA) to the potential landscape, systematically identifying major spatiotemporal patterns. By implementing this two-step reduction method, we reveal significant shifts during a pandemic, characterized by an overall declines in mobility and stark contrasts between weekdays and holidays. These findings underscore the effectiveness of our framework in uncovering complex mobility patterns and provide valuable insights into urban planning and public health interventions.

Keywords: Human mobility, potential landscape, principal component analysis, mobility patterns, COVID-19 pandemic

1 Introduction

Humans are inherently mobile beings who frequently travel from one location to another for various daily activities, such as commuting, shopping, entertainment, and education. These individual movements collectively shape the intricate dynamics of urban mobility. Spatiotemporal patterns of human flow are crucial for a wide range of applications, including controlling the spread of epidemics [1–3], understanding social and economic issues such as social segregation [4–6] and urban gender disparities [7, 8], and integrating public transportation systems with urban design plans to enhance mobility efficiency [9–12].

Human flow is not static but fluctuates dynamically over time. Therefore, understanding the evolution of these patterns is crucial. For example, on weekdays, cities exhibit distinct human flow patterns during morning and evening rush hours, whereas on weekends, movement trends differ significantly. Furthermore, external factors such as natural disasters and pandemics can drastically alter these patterns. Natural disasters, such as earthquakes or floods, can abruptly disrupt natural human movement, triggering mass evacuations or substantial changes in commuting behaviors. Similarly, the outbreak of a pandemic, such as Coronavirus Disease 2019 (COVID-19) [13], can cause unprecedented shifts in human mobility, with lockdowns and travel restrictions drastically reducing movement and reshaping human flow patterns on a global scale. These temporal variations in human flow result from a complex interplay of factors, including economic activity, social events, environmental conditions, and policy interventions. Examining these patterns over time provides valuable insights into the underlying mechanisms driving human mobility.

Recent advancements in data collection and processing technologies have enabled the analysis of large-scale mobility data at high spatiotemporal resolutions, facilitating the exploration of dynamic mobility patterns and the identification of underlying structures in human flow. We live in an era where vast amounts of human mobility data are generated from various sources [14–18]. Traditionally, mobility data have been gathered through censuses and surveys that collect information on where people live and work. With the increasing prevalence of mobile phones, call detail records (CDRs) have become an important data source. These records, provided by mobile network operators, track the location of a signal tower when a phone call or text

message is sent. Additionally, global positioning system (GPS) data collected from GPS-enabled devices and smartphones offer increasingly detailed location information. Social media platforms also contribute valuable mobility data through user interactions and geotagged posts.

Despite the availability of vast amounts of data, understanding the spatiotemporal patterns of human flow remains challenging owing to the large volume and complexity of such data. In previous research, mobility data have often been reduced down to temporal trends of macroscopic statistics, such as displacement and waiting time distributions [19], radius of gyration [20], number of visited places and visitation frequency [21], predictability [22], motifs [23], and mobility synchronization [24]. Some studies have examined the dynamics of one or more of these metrics [24–31], revealing common patterns in human mobility. However, these data processing approaches often mitigate information overload by reducing detail, resulting in the loss of location-specific information. In other instances, data have been transformed into spatial distributions of temporal populations [32–34], preserving location-specific details but losing crucial mobility information, such as trip distances and their origins. Additionally, data have been used to fit general models of human mobility, including the gravity model [35], the intervening opportunities model [36–40], the radiation model [41–49], and the exploration and preferential return (EPR) model [21, 50–54]. Although these models offer valuable insights, systematic examination of the dynamics of human mobility patterns across different contexts is limited. In summary, previous approaches have failed to retain the full complexity of human mobility data. Methods that aggregate data into macroscopic statistics often lose spatial specificity, whereas those emphasizing spatial distributions omit essential trip information, such as origins and distances. Furthermore, model-based approaches abstract real-world patterns to fit theoretical constructs, which may not fully capture the intricacies of human movement.

To address those existing issues, this study proposes a two-step reduction method for human mobility data, enabling the effective visualization of spatiotemporal patterns in human flow (Fig. 1). As shown in the middle panel of Fig. 1, the first step involves utilizing the concept of the potential landscape of human flow [55–59]. In our case, the potential landscape is generated through applying the combinatorial Hodge theory [60–63] to the origin-destination (OD) matrix. This method offers several advantages such as significantly reducing data dimensionality by transforming an OD matrix with N^2 elements for N regions of interest into a potential landscape with only N elements. Despite the reduction, human flow can still be accurately reproduced [55]. Furthermore, the potential landscape quantifies the relational mobility information between locations as location-level statistics, which can be naturally visualized on a map. This quantification facilitates the comparison of mobility patterns across different spatial scales. Accordingly, this study investigates the temporal evolution of human flow patterns. In the second step, the spatiotemporal dynamics of the potential landscape are categorized into spatial and temporal components using principal component analysis (PCA). PCA is a widely used statistical technique for dimensionality reduction in data analysis. Previous research has employed PCA to analyze and interpret human mobility patterns [64–67]. By applying PCA to the time series of the potential landscape, as shown in the right panel of Fig. 1, the temporal trajectory of

the score on the principal component axes is extracted, representing the contribution of each spatial grid to the corresponding eigenvector \mathbf{w}_k . This study investigates the spatiotemporal patterns of human mobility by constructing a scalar potential field for human flow and analyzing its temporal evolution. The findings reveal significant shifts in mobility behavior during the pandemic, including decreased overall movement and high spatially-constrained mobility patterns, particularly during peak commute hours. Additionally, a clear difference is observed between weekday and holiday mobility, with holidays showing delayed peaks and less spatial dispersion, both before and during the pandemic.

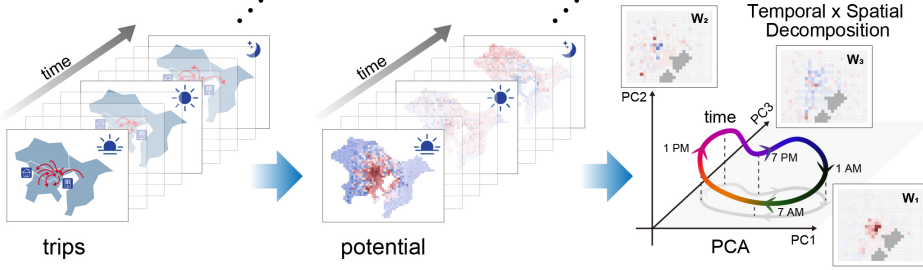


Fig. 1: Methodology for examining spatiotemporal mobility patterns. (Left) Raw, hourly OD data derived from mobility datasets serve as the foundation of the analysis, capturing detailed flow patterns between spatial grids. (Middle) Hourly OD data transformed into a series of hourly potential landscapes. (Right) Principal component axes representing the contribution of each spatial grid to the corresponding eigenvector \mathbf{w}_k . Hourly dynamics are represented by the trajectory of score changes over time.

The remainder of this paper is organized as follows: Section 2 describes the mobility dataset, which contains hourly OD information for both pre-COVID-19 and COVID-19 periods. Section 3 provides an overview of combinatorial Hodge theory (Sec. 3.1) and explains its application to human flow data (Sec. 3.2). In Sec. 4, we begin with the extraction of the scalar potential field of human flow through the unique decomposition of a given OD matrix using combinatorial Hodge theory. Then, PCA is applied to the potential landscape to investigate temporal variations in human flows within a 24-hour period across different scenarios, including weekday versus weekend trips and pre-COVID-19 versus during COVID-19 periods. Finally, Section 5 summarizes our key findings and concludes the paper. These results highlight the profound impact of COVID-19 on urban mobility and provide insights into human flow adaptations to external disruptions, thereby offering valuable implications for urban planning and public health policies.

2 Data

For this study, we use Japanese human mobility data, “LocationMind xPop”, provided by LocationMind Inc. [68], which encompasses GPS records collected within the Tokyo metropolitan area. The dataset covers two time periods: May and June 2019 (pre-COVID-19) and May and June 2021 (during COVID-19). These data include estimated home locations, origins, and destinations, mapped using a 2km by 2km spatial grid system based on the Japanese mesh index [69]. The dataset distinguishes between weekday and holiday movements and records the specific hours during which these movements occurred. Notably, the data are aggregated, reflecting the average flow volumes over multiple days rather than individual trips. Additionally, the number of trips is based on the unique users recorded, with adjustments relative to the population census data, providing an estimate of real population movements.

The “LocationMind xPop” data refer to human flow data collected from individual location information transmitted by smartphones with users’ consent, provided by NTT DOCOMO, INC. To ensure privacy, the data provider processed the data collectively and statistically, protecting any personally identifiable information. The original location data comprised GPS coordinates (latitude and longitude) recorded at a frequency as short as every 5 minutes and did not include any information that could directly identify individuals.

The background map layouts in Figs. 2 and 3 are based on data by © OpenStreetMap contributors, available under the Open Database License (ODbL). Map tiles by © CARTO. The results in Figs. 2, 3, 4, and 5 were obtained by using data “LocationMind xPop © LocationMind Inc” [68].

3 Methods

3.1 Combinatorial Hodge theory

To extract essential insights from human mobility data, we apply combinatorial Hodge theory [60–62], a mathematical framework that decomposes a given vector field into three orthogonal components: the gradient of a scalar potential field, the curl of a vector potential field, and a harmonic component. When used in the analysis of human mobility data, this approach provides a structured method for examining the OD matrix, which represents the movement of individuals between locations [55, 56]. By introducing a scalar potential field through this decomposition, we effectively visualize the spatial distribution of human flow, reveal latent mobility patterns, and gain a deeper understanding of the underlying dynamics.

The potential landscape is derived using combinatorial Hodge theory [60–62] on an undirected graph $G(V, E)$, where V denotes a set of vertices and E represents a set of edges. Edge flow Y is assigned to each edge, with each element Y_{ij} representing the flow from vertex i to vertex j . The edge flow is skew-symmetric, i.e., $Y_{ij} = -Y_{ji}$. The combinatorial gradient, curl, and divergence are defined as follows [62]:

$$(\text{grad } s)(i, j) = s_j - s_i \quad \text{for } \{i, j\} \in E, \quad (1)$$

$$(\text{curl } Y)(i, j, k) = Y_{ij} + Y_{jk} + Y_{ki} \quad \text{for } \{i, j, k\} : \{i, j\}, \{j, k\}, \{k, i\} \in E, \quad (2)$$

$$(\operatorname{div} Y)(i) = \sum_{j \text{ s.t. } \{i,j\} \in E} Y_{ij}, \quad (3)$$

where s denotes the potential to be introduced.

The space of edge flow \mathcal{Y} is orthogonally decomposed into the images and kernels of these operators:

$$\mathcal{Y} = \operatorname{im}(\operatorname{grad}) \oplus \ker(\Delta_1) \oplus \operatorname{im}(\operatorname{curl}^*), \quad (4)$$

where $\ker(\Delta_1) = \ker(\operatorname{curl}) \cap \ker(\operatorname{div})$ and curl^* is the adjoint operator of the curl .

Potential s is defined as the solution to the weighted least-squares optimization problem given by:

$$\min_s \sum_{\{i,j\} \in E} W_{ij} [(\operatorname{grad} s)(i,j) - Y_{ij}]^2 = \min_s \sum_{\{i,j\} \in E} W_{ij} [(s_j - s_i) - Y_{ij}]^2, \quad (5)$$

where $W_{ij} (\in [0, 1])$ is the weight of pairwise comparison, primarily determined by the distance d_{ij} as discussed in Sec. 3.2. The optimization problem determines the closest point to the given data Y in the subspace of edge flows, which comprise the gradient flows of the potential. The problem can be solved by an l_2 -projection of Y onto $\operatorname{im}(\operatorname{grad})$. With a Euclidean inner product in space \mathcal{Y} , $\langle X, Y \rangle = \sum_{\{i,j\} \in E} W_{ij} X_{ij} Y_{ij}$, the normal equation can be expressed as:

$$\Delta_0 s = -\operatorname{div} Y, \quad (6)$$

where Δ_0 is the graph Laplacian defined by:

$$[\Delta_0]_{ij} = \begin{cases} \sum_j W_{ij} & \text{if } i = j \\ -W_{ij} & \text{if } \{i, j\} \in E \\ 0 & \text{otherwise.} \end{cases} \quad (7)$$

Finally, the potential s is given by the minimal-norm solution of Eq. 6 as:

$$s = -\Delta_0^\dagger \operatorname{div} Y, \quad (8)$$

where \dagger denotes the Moore-Penrose inverse.

3.2 Application of combinatorial Hodge theory to mobility flow

For a given OD matrix M representing the mobility flow, we assign edge flow Y by calculating the net flow as:

$$Y = M - M^\top, \quad (9)$$

where the element Y_{ij} denotes the net flow from i to j , satisfying the necessary skew-symmetric condition in the combinatorial Hodge theory [60–62]. To define the potential using the optimization problem in Eq. 5, the regional difference in potential, $s_j - s_i$,

is evaluated in comparison to the net flow Y_{ij} , but only for location pairs included in the edge set E . This evaluation is further weighted using W_{ij} , which reflects the significance of each pair in the analysis.

The determination of edges E and weights W_{ij} is strongly influenced by the distances between locations. To explore the dependence of mobility flow on distance, we analyze the percentage of non-zero mobility pairs ($M_{ij} > 0$ or $M_{ji} > 0$) as a function of road distance, using data from the Japanese mobility dataset (Sec. 2). The results are presented in the Supplementary Information. Our analysis revealed a sharp decline in the percentage of non-zero mobility pairs as the distance increases. Notably, even at a relatively short distance of approximately $d_{ij} \sim 40$ km, nearly half of the mobility pairs exhibit zero flow volume.

The phenomenon of zero-mobility flow offers several important implications. Mobility incurs substantial costs, and zero flow suggests that the costs associated with travel outweigh the driving forces behind regional differences. At shorter distances, where travel costs are generally low, zero mobility flow between two locations implies that the regional difference ($s_j - s_i$) is minimal. Conversely, at longer distances, where costs become disproportionately high, the absence of mobility flow conveys little useful information about regional potential differences.

To address this issue, we apply a weighting method to systematically exclude trips that occur at distances where mobility is rarely observed. This method, which has been proven to perform well in urban settings [56], enabling us to define a threshold distance, denoted as θ . The threshold θ is established as the distance below which the majority of trips occur, based on the probabilistic criterion $p(X < \theta) = 0.99$ (Supplementary Information). Specifically, the weight W_{ij} is expressed as:

$$W_{ij} = \begin{cases} 1 & \text{mobility pair } \{(i, j) \mid d_{ij} > \theta\} \\ 0 & \text{mobility pair } \{(i, j) \mid d_{ij} < \theta\} \end{cases}. \quad (10)$$

For the set of edges E , we select pairs with positive weights, $\{(i, j) \mid W_{ij} = 1\}$.

By applying combinatorial Hodge theory to the OD matrix, we transform the data as illustrated in Fig. 1, progressing from the left to the middle panel. Specifically, the OD information at each time step is decomposed into a one-dimensional scalar field, referred to as a potential landscape [55, 56]. This potential landscape serves as a compact yet powerful representation of spatial dynamics, preserving essential spatial information while reducing data dimensionality. Each spatial grid is assigned a unique potential value that encapsulates the relative attractiveness or activity level of the location. Notably, the potential landscape retains the key trip information encoded in the OD matrix. This preservation is achieved because the difference between potential values at two locations determines the likelihood and direction of trips. Individuals tend to move from areas of lower potential to areas of higher potential, aligning with the intuitive interpretation of flows driven by regional differences in potential.

3.3 Principal component analysis (PCA)

PCA is a statistical technique widely used for dimensionality reduction in data analysis. It transforms a high-dimensional dataset into a lower-dimensional set of linearly

uncorrelated components that capture the maximum variance in the original data. In this study, we aim to understand patterns in human mobility data by applying PCA to the potential landscape of human flow. Our objective is to identify the positions of spatial grids within the potential landscape and examine how the principal components contribute to the temporal evolution of human flow patterns.

Consider a dataset represented by a matrix \mathbf{X} with n rows and p columns. Each row r , denoted as $\mathbf{x}^{(r)}$, is a vector representing one observation of data with p features. The data matrix \mathbf{X} has column-wise zero empirical means, suggesting that the sample mean of each column has been shifted to zero. In this case, \mathbf{X} represents the series of potentials across spatial grids, where p is the number of spatial grids, and n is the number of observations under various conditions. Specifically, $n = 96$ captures data for 24 hours across different scenarios: weekdays in 2019, holidays in 2019, weekdays in 2021, and holidays in 2021. For example, a particular column may represent the potential at 08:00 on weekdays in 2019.

The primary goal of PCA is to identify features that explain most of the variance in the data. First, we calculate the covariance matrix \mathbf{Q} of the dataset \mathbf{X} as:

$$\mathbf{Q} = \frac{1}{n-1} \sum_{r=1}^n (\mathbf{x}^{(r)})^\top \mathbf{x}^{(r)} = \frac{1}{n-1} \mathbf{X}^\top \mathbf{X}. \quad (11)$$

Performing eigenvalue decomposition on \mathbf{Q} yields a set of eigenvalues $\lambda_1, \lambda_2, \dots, \lambda_p$ and their corresponding eigenvectors $\mathbf{w}_1, \mathbf{w}_2, \dots, \mathbf{w}_p$. The eigenvectors \mathbf{w}_k represent the directions in the feature space along which the data varies the most, while the eigenvalues λ_k indicate the amount of variance captured by each corresponding eigenvector \mathbf{w}_k . The transformation is thereby performed as follows:

$$\text{PC}_k^{(r)} = \mathbf{x}^{(r)} \cdot \mathbf{w}_k \quad \text{for } r = 1, \dots, n \quad \text{and } k = 1, \dots, l, \quad (12)$$

where $\text{PC}_k^{(r)}$ is defined as the k -th principal component *score* of the data point in row r . For this study, we specifically denote these scores as PC1, PC2, PC3, and so on. Notably, the original data points $\mathbf{x}^{(r)}$ can be reconstructed from these principal components as follows:

$$\mathbf{x}^{(r)} = \sum_{k=1}^l \text{PC}_k^{(r)} \mathbf{w}_k, \quad (13)$$

which explicitly demonstrates PCA as a linear transformation that decomposes the mobility data into temporal components $\text{PC}_k^{(r)}$ and spatial patterns \mathbf{w}_k .

The k -th eigenvalue λ_k is equal to the sum of the squares of the scores over the n observations. It is expressed as:

$$\lambda_k = \sum_{i=1}^n (\text{PC}_k^{(r)})^2 = \sum_{i=1}^n (\mathbf{x}^{(r)} \cdot \mathbf{w}_k)^2. \quad (14)$$

In this study, we analyze the eigenvectors and principal components scores to interpret the outcomes of PCA and their implications for human mobility patterns.

As illustrated in Fig. 1 (right panel), PCA decomposes the potential landscape into distinct spatial and temporal dimensions. The axes PC1, PC2, and PC3 represent the spatial contributions of each principal direction, denoted by the eigenvector \mathbf{w}_k . The temporal evolution of mobility is captured through colored trajectories that depict the hourly variation in the principal component scores.

4 Results

4.1 Temporal evolution of potential landscape

Using Japanese human mobility data (Sec. 2), we first calculated the potential landscape of human flow at different hours of the day. The results for weekdays in 2019 are presented in Fig. 2, displaying the spatial landscape at 3-hour intervals (hourly details are provided in the Supplementary Information). In these maps, the Yamanote railway loop is represented by a green line enclosing the Tokyo urban core, interlinking major centers such as Shinjuku, Shibuya, Ikebukuro, Ueno, and Tokyo Station. Areas beyond the loop primarily correspond to suburban regions and nearby cities.

During the morning rush hours, from 06:00 (Fig. 2c) to 09:00 (Fig. 2d), the potential values in the central area were markedly positive, whereas several grids in the peripheral areas exhibited negative potential values. This pattern reflected the significant movement of estimated commuters from residential zones to the central business district, where a high concentration of workplaces were located. The pronounced central attractiveness observed during these hours aligned with typical commuting patterns.

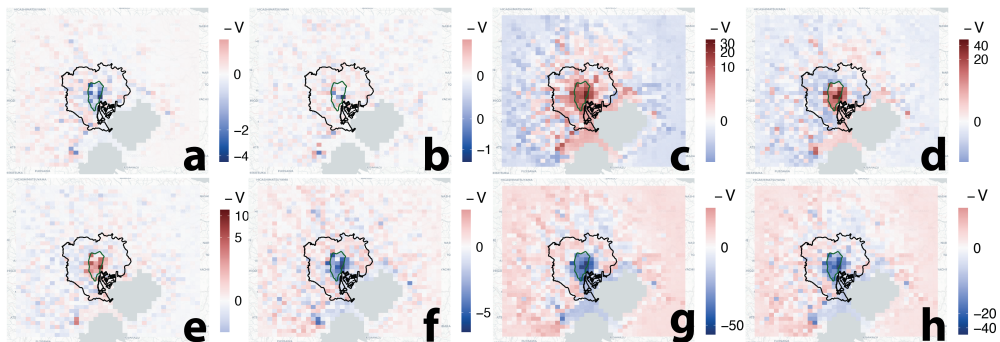


Fig. 2: Time evolution of the potential landscape $-V (= s)$ for weekdays in 2019 in the Tokyo metropolitan area. Color codes represent the potential value in each spatial grid. Black contour lines delineate the borders of Tokyo's special wards (Tokyo Metropolis), marking the primary urban center. Green contour lines denote the Yamanote railway loop, which encloses the city's urban core. Subfigures correspond to different hours: (a) 00:00; (b) 03:00; (c) 06:00; (d) 09:00; (e) 12:00; (f) 15:00; (g) 18:00; (h) 21:00.

In the evening hours at approximately 18:00 (Fig. 2g), the peripheral areas exhibited distinctly positive potential values, while the urban core displayed negative values.

This pattern marked the end of the workday and the outward movement of individuals from central workplaces as they returned to their residential areas. The trend persisted into the late evening (Fig. 2h), with negative potential values remaining in the central areas and positive values prevailing in the periphery. These trends also reflected post-work activities, such as social gatherings, before individuals returned home. These findings align with well-established commuting dynamics in urban environments, underscoring the utility of potential landscapes in capturing fundamental patterns of human mobility.

4.2 Spatiotemporal dynamics revealed through PCA on potential landscape

Further, we performed PCA on the potential landscapes for different scenarios, including weekdays and holidays in 2019 and 2021 (Sec. 3.3). Notably, the first three principal components accounted for 96.3% of the variance (Supplementary Information), underscoring their crucial role in explaining the underlying mobility patterns. By focusing on these dominant components, we transformed the temporal sequence of potential landscapes into a trajectory within the three-dimensional space of the principal components. As illustrated in the right panel of Fig. 1, this trajectory encoded temporal information, while the corresponding eigenvectors \mathbf{w}_k conveyed the spatial characteristics of the flow. The results for weekdays in 2019 are shown in Fig. 3.

PC1 primarily captured the characteristic commuting patterns, with its score peaking during the morning rush hours (06:00-09:00) and dipping in the evening (17:00-22:00), as shown in Fig. 3a. The corresponding eigenvector \mathbf{w}_1 (Fig. 3d) was concentrated within the special wards of Tokyo, particularly inside the Yamanote loop line, which constituted the city's central business district and extended to several key subcenters including Chiba, Kawasaki, and Yokohama. This spatial distribution, combined with the temporal trend, signified the typical flow of estimated commuters from suburban regions into urban centers in the morning, followed by return trips in the evening. Notably, PC1 consistently exhibited higher scores than PC2 and PC3, underscoring its primary role in capturing dominant mobility dynamics.

PC2 reflected commuting behavior but exhibited more localized spatiotemporal characteristics. Its score peaked at approximately 08:00 and dropped between 17:00 and 18:00 (Fig. 3a). The eigenvector \mathbf{w}_2 (Fig. 3e) was positively concentrated around Tokyo Station and Shinagawa Station—both major high-speed rail hubs—and negatively concentrated around terminal stations such as Ikebukuro, Shinjuku, Kawasaki, Funabashi, and Yokohama. These terminals are positioned along multiple radial lines extending from Tokyo Station. Consequently, PC2 primarily reflected flows from these subcenter regions toward central high-speed rail hubs in the morning, followed by return trips in the early evening.

Contrarily, PC3 exhibited a distinct temporal pattern, declining from 06:00 to 07:00 before sharply increasing between 08:00 and 10:00 (Fig. 3a). The eigenvector \mathbf{w}_3 (Fig. 3f) was predominantly positive in suburban areas and negative in central districts, with isolated positive hotspots near Tokyo and Yokohama Stations. These findings suggested that PC3 served as a complementary modulation to the commuting flows captured by PC1 and PC2, particularly reflecting movements toward or from key

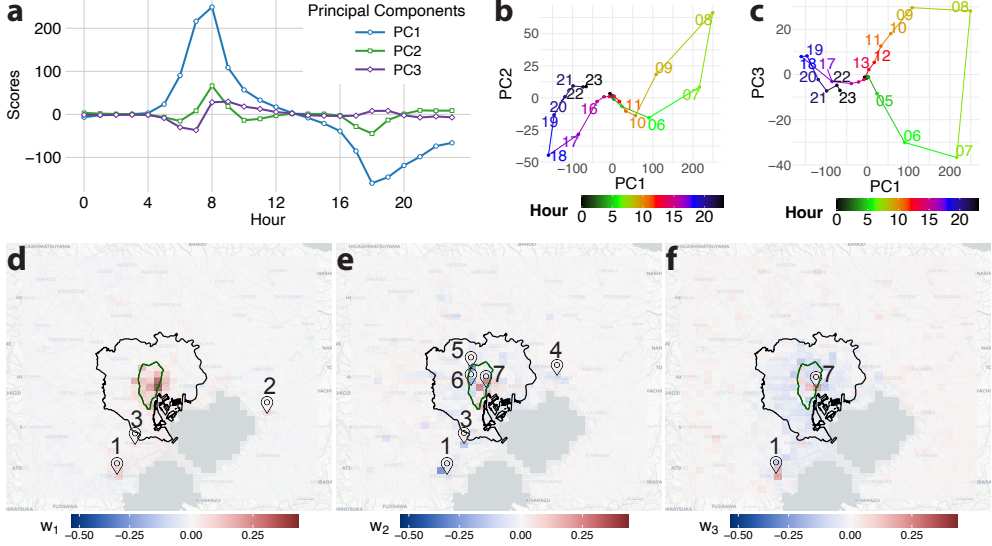


Fig. 3: Temporal evolution of the PC1, PC2, and PC3 scores, along with their corresponding eigenvectors on weekdays in 2019. (a) Time series of the principal component scores over 24-hour period. (b) and (c) Relationships between principal components in PC2 vs. PC1 and PC3 vs. PC1 spaces, respectively. The corresponding eigenvectors are illustrated in (d) w_1 , (e) w_2 , and (f) w_3 . Numbers in the maps (d)-(f) indicate key locations: 1-Yokohama, 2-Chiba, 3-Kawasaki, 4-Funabashi, 5-Ikebukuro, 6-Shinjuku, and 7-Tokyo station. Contour lines match those in Fig. 2.

rail hubs and surrounding areas during morning hours. Furthermore, PC3 exhibited smoother yet more frequent variations throughout the day, capturing midday activity and smaller-scale movements, such as work-related travel, thereby contributing to the overall daily mobility patterns.

4.3 Comparison of human mobility patterns across scenarios

Compared with the time series of potential landscapes, the PCA-based representation offered a macroscopic view of spatiotemporal patterns through a compact set of principal components. As shown in Fig. 3, the trajectory in principal component space encoded the temporal signatures of these patterns. We compared the trajectories across different conditions—weekdays vs. weekends and 2019 vs. 2021—within the same three-dimensional space, enabling a systematic comparison of mobility trends.

The weekday and holiday score trajectories for 2019 are shown in Fig. 4, highlighting distinct temporal signatures. As discussed in Sec. 4.2, PC1 and PC3 captured weekday commuting flows and complementary movements. On holidays, PC1 followed a similar trajectory to weekdays, as shown in Fig. 4a, but with a lower overall amplitude and a peak occurring 1 hour later. The scores of PC3 exhibited a similar tendency, as shown in Fig. 4c. These findings indicated that commuting-like travel persisted on holidays but with reduced intensity and a later start compared to weekdays.

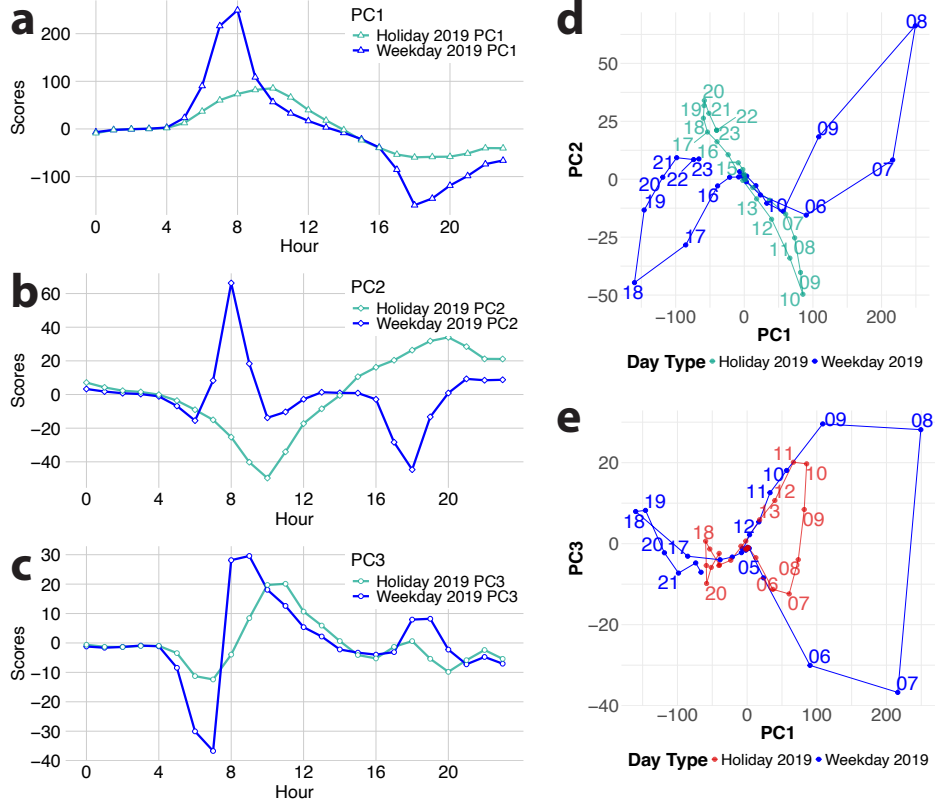


Fig. 4: Comparison of weekday and holiday trajectories for 2019 in the principal component space. (a)-(c) Time evolution of PC1, PC2, and PC3 scores, respectively. (d) Trajectories projected in the PC1-PC2 plane. (e) Trajectories projected in the PC1-PC3 plane.

PC2 exhibited markedly different behaviors on holidays than on weekdays. As shown in Fig. 4b, PC2 score was negative during holiday mornings (07:00-12:00) and positive in the evening (16:00-23:00), whereas on weekdays, PC2 score was positive in mornings and negative in the evening. This opposite trend in PC2 scores on holidays captured flows originating from central bullet train stations toward suburban terminals along radial lines, reversing the weekday flow pattern. Moreover, Figure 4b shows notable temporal differences in PC2 between weekdays and holidays. On weekdays, PC2 peaked sharply at approximately 08:00, while on holidays, it exhibited a broad dip from 07:00 to 12:00, reaching a minimum near 10:00. A similar shift was observed in the evening, with extended activity periods. These findings suggested that on holidays, PC2 primarily reflected leisure and entertainment trips rather than weekday commuting flows.

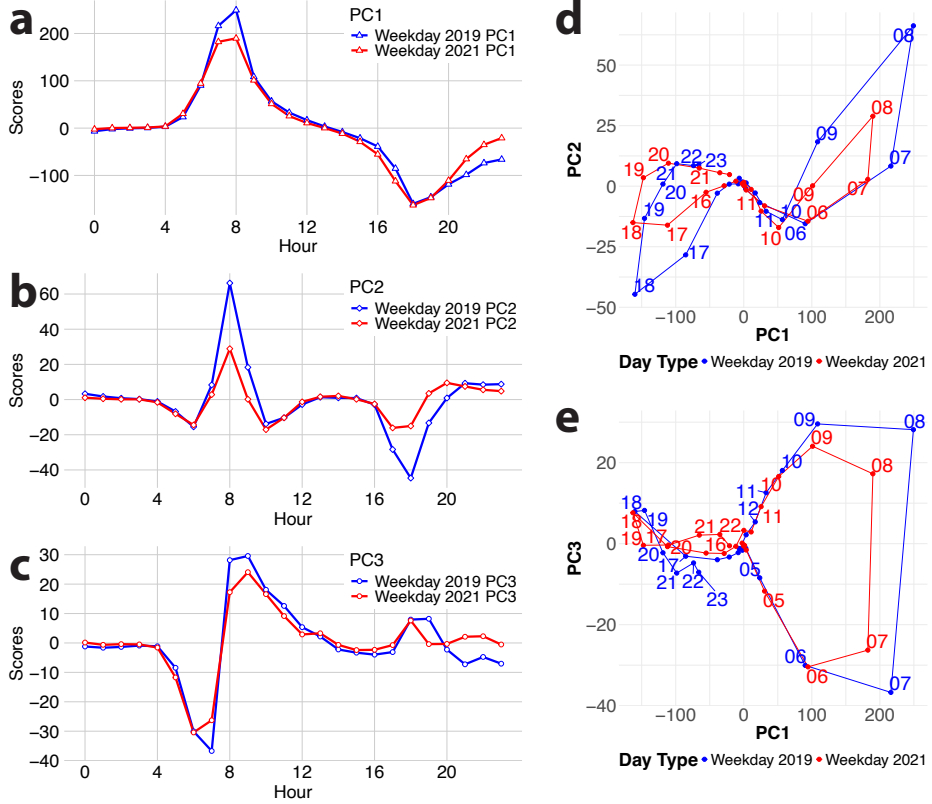


Fig. 5: Comparison of 2019 and 2021 trajectories for weekdays in the principal component space. (a)-(c) Time evolution of PC1, PC2, and PC3 scores, respectively. (d) Trajectories projected in the PC1-PC2 plane. (e) Trajectories projected in the PC1-PC3 plane.

Further, we compared mobility trajectories before and during the COVID-19 pandemic. The weekday trajectories for 2019 and 2021 are shown in Fig. 5. Although both trajectories shared a similar overall shape—indicating that the fundamental structure of mobility patterns remained largely unchanged—the 2021 trajectory exhibited noticeably lower amplitudes during peak hours. For example, morning peaks in PC1 and PC2 were smaller (Fig. 5a-c), and the evening return-trip dip in PC2 was also reduced and ended earlier. Contrarily, the amplitude differences at other times of the day were less pronounced.

During the data collection period (May and June 2021), the Japanese government declared a state of emergency in Tokyo to curb COVID-19 resurgence ahead of the 2021 Tokyo Summer Olympics. Although Japan's mobility restrictions were relatively lenient compared to international measures, prior research documented an overall decline in metropolitan mobility [70, 71]. Our findings further revealed that these

restrictions primarily reduced mobility during peak commuting hours, whereas daily movement patterns outside these periods remained relatively unchanged.

5 Discussion

This study systematically investigates human mobility patterns in the Tokyo metropolitan area using a proposed analytical framework based on potential landscape and PCA. By comparing behaviors across distinct contexts, we identify clear distinctions in movement dynamics. Our method effectively captures differences in daily mobility patterns between weekdays and holidays, and reveals significant changes in mobility behavior during the COVID-19 pandemic. These findings provide a comprehensive understanding of how human mobility adapts to external factors, such as public health crises, across both temporal and spatial dimensions. Notably, the proposed approach leverages the potential landscape framework to represent and analyze the dynamics of human flow. This method serves as a powerful tool for visualizing mobility patterns by capturing the temporal evolution of spatial potential distributions. Mapping these shifts onto a dynamic landscape reveals intricate variations in behavior, such as constrained mobility during peak hours in 2021 and notable differences in holiday and weekday movements. Unlike static mobility data, the proposed approach offers deeper insight into the response of human movements to routine activities and external disruptions.

However, this study has several limitations. First, we relied on aggregated two-month mobility averages for 2019 and 2021, which restricted our ability to detect transient fluctuations, such as those driven by weather, short-term events, or sudden policy shifts. Second, we adjusted the GPS data using population census information, assuming proportional relationships between the sampled device users and the broader population. This assumption may overlook potential variations in local population density and disparities in device usage, thereby introducing bias. Furthermore, although the proposed method reproduced broad flow tendencies between regions, specific OD pair information was not retained. Such granularity can be critical for transportation planning, where absolute flow volumes between specific OD pairs are often essential.

Nonetheless, the proposed method provides a macroscopic view of spatiotemporal mobility patterns, making it well-suited for applications that do not require a high level of detail. Our findings have direct relevance for various applications. A deeper understanding of mobility patterns can inform urban planning, support the design of optimized transportation networks, and guide the allocation of public resources. From a public health perspective, insights from potential landscapes can help policymakers develop targeted interventions during pandemics and other crises. Additionally, the potential landscape approach provides policymakers a dynamic tool for tracking mobility trends, enabling them to adjust infrastructure and regulations in response to evolving urban needs. Future studies with higher temporal resolution and real-time data are essential for expanding the scope of these applications and enhancing the precision of mobility analyses.

Statements and Declarations

Competing Interests

The authors declare that they have no competing interests.

Data Availability Statement

The mobility flow data for Japan utilized in this study is available for purchase from LocationMind Inc., a Japanese company [68] (For inquiries, use their contact form [72]). The data product is called “LocationMind xPop.”

Acknowledgements

Y.D. is supported by JST SPRING, Grant Number JPMJSP2114. T.A. is supported by JSPS KAKENHI Grant Number JP24K07699, and JSPS KAKENHI Grant Number JP24H01473. N.F. is supported by JSPS KAKENHI Grant Number JP24K03007, and JST PRESTO Grant Number JPMJPR21RA, Japan. This work additionally receives support from the Research Institute for Mathematical Sciences, an International Joint Usage/Research Center located in Kyoto University.

References

- [1] Jia, J.S., Lu, X., Yuan, Y., Xu, G., Jia, J., Christakis, N.A.: Population flow drives spatio-temporal distribution of COVID-19 in China. *Nature* **582**, 389–394 (2020)
- [2] Viboud, C., Bjørnstad, O.N., Smith, D.L., Simonsen, L., Miller, M.A., Grenfell, B.T.: Synchrony, waves, and spatial hierarchies in the spread of influenza. *Science* **312**, 447–451 (2006)
- [3] Hazarie, S., Soriano-Paños, D., Arenas, A., Gómez-Gardeñes, J., Ghoshal, G.: Interplay between population density and mobility in determining the spread of epidemics in cities. *Communications Physics* **4**, 191 (2021)
- [4] Amini, A., Kung, K., Kang, C., Sobolevsky, S., Ratti, C.: The impact of social segregation on human mobility in developing and industrialized regions. *EPJ Data Science* **3**, 1–20 (2014)
- [5] Moro, E., Calacci, D., Dong, X., Pentland, A.: Mobility patterns are associated with experienced income segregation in large us cities. *Nature Communications* **12**, 4633 (2021)
- [6] Yang, Y., Pentland, A., Moro, E.: Identifying latent activity behaviors and lifestyles using mobility data to describe urban dynamics. *EPJ Data Science* **12**, 15 (2023)

- [7] Gauvin, L., Tizzoni, M., Piaggesi, S., Young, A., Adler, N., Verhulst, S., Ferres, L., Cattuto, C.: Gender gaps in urban mobility. *Humanities and Social Sciences Communications* **7**, 1–13 (2020)
- [8] Collins, T., Di Clemente, R., Gutiérrez-Roig, M., Botta, F.: Spatiotemporal gender differences in urban vibrancy. *Environment and Planning B: Urban Analytics and City Science*, 23998083231209073 (2023)
- [9] Vazifeh, M.M., Santi, P., Resta, G., Strogatz, S.H., Ratti, C.: Addressing the minimum fleet problem in on-demand urban mobility. *Nature* **557**, 534–538 (2018)
- [10] Xu, Y., Clemente, R.D., González, M.C.: Understanding vehicular routing behavior with location-based service data. *EPJ Data Science* **10**, 1–17 (2021)
- [11] Bongiorno, C., Zhou, Y., Kryven, M., Theurel, D., Rizzo, A., Santi, P., Tenenbaum, J., Ratti, C.: Vector-based pedestrian navigation in cities. *Nature Computational Science* **1**, 678–685 (2021)
- [12] Gallotti, R., Porter, M.A., Barthelemy, M.: Lost in transportation: Information measures and cognitive limits in multilayer navigation. *Science Advances* **2**, 1500445 (2016)
- [13] Zhu, N., Zhang, D., Wang, W., Li, X., Yang, B., Song, J., Zhao, X., Huang, B., Shi, W., Lu, R., Niu, P., Zhan, F., Ma, X., Wang, D., Xu, W., Wu, G., Gao, G.F., Tan, W.: A novel coronavirus from patients with pneumonia in China, 2019. *New England Journal of Medicine* **382**, 727–733 (2020)
- [14] Blondel, V.D., Decuyper, A., Krings, G.: A survey of results on mobile phone datasets analysis. *EPJ Data Science* **4**, 1–55 (2015)
- [15] Zheng, Y.: Trajectory data mining: an overview. *ACM Transactions on Intelligent Systems and Technology (TIST)* **6**, 1–41 (2015)
- [16] Zhao, K., Tarkoma, S., Liu, S., Vo, H.: Urban human mobility data mining: An overview. In: 2016 IEEE International Conference on Big Data (Big Data), pp. 1911–1920 (2016)
- [17] Zhu, L., Yu, F.R., Wang, Y., Ning, B., Tang, T.: Big data analytics in intelligent transportation systems: A survey. *IEEE Transactions on Intelligent Transportation Systems* **20**, 383–398 (2018)
- [18] Yabe, T., Jones, N.K., Rao, P.S.C., Gonzalez, M.C., Ukkusuri, S.V.: Mobile phone location data for disasters: A review from natural hazards and epidemics. *Computers, Environment and Urban Systems* **94**, 101777 (2022)
- [19] Brockmann, D., Hufnagel, L., Geisel, T., Geisel, T.: The scaling laws of human

travel. *Nature* **439**, 462–465 (2006)

[20] González, M.C., Hidalgo, C.A., Barabási, A.-L.: Understanding individual human mobility patterns. *Nature* **453**, 779–782 (2008)

[21] Song, C., Koren, T., Wang, P., Barabási, A.-L.: Modelling the scaling properties of human mobility. *Nature Physics* **6**, 818–823 (2010)

[22] Song, C., Qu, Z., Blumm, N., Barabási, A.-L.: Limits of predictability in human mobility. *Science* **327**, 1018–1021 (2010)

[23] Schneider, C.M., Belik, V., Couronné, T., Smoreda, Z., González, M.C.: Unravelling daily human mobility motifs. *Journal of The Royal Society Interface* **10**, 20130246 (2013)

[24] Santana, C., Botta, F., Barbosa, H., Privitera, F., Menezes, R., Di Clemente, R.: COVID-19 is linked to changes in the time–space dimension of human mobility. *Nature Human Behaviour* **7**, 1729–1739 (2023)

[25] Kraemer, M.U., Sadilek, A., Zhang, Q., Marchal, N.A., Tuli, G., Cohn, E.L., Hswen, Y., Perkins, T.A., Smith, D.L., Reiner Jr, R.C., *et al.*: Mapping global variation in human mobility. *Nature Human Behaviour* **4**, 800–810 (2020)

[26] Hasan, S., Schneider, C.M., Ukkusuri, S.V., González, M.C.: Spatiotemporal patterns of urban human mobility. *Journal of Statistical Physics* **151**, 304–318 (2013)

[27] Lu, X., Bengtsson, L., Holme, P.: Predictability of population displacement after the 2010 Haiti earthquake. *Proceedings of the National Academy of Sciences* **109**, 11576–11581 (2012)

[28] Geng, W., Yang, G.: Partial correlation between spatial and temporal regularities of human mobility. *Scientific Reports* **7**, 6249 (2017)

[29] Wang, Q., Taylor, J.E.: Patterns and limitations of urban human mobility resilience under the influence of multiple types of natural disaster. *PLoS one* **11**, 0147299 (2016)

[30] Heiler, G., Reisch, T., Hurt, J., Forghani, M., Omani, A., Hanbury, A., Karimipour, F.: Country-wide mobility changes observed using mobile phone data during COVID-19 pandemic. In: 2020 IEEE International Conference on Big Data (big Data), pp. 3123–3132 (2020)

[31] Kalleitner, F., Schiestl, D.W., Heiler, G.: Varieties of mobility measures: Comparing survey and mobile phone data during the COVID-19 pandemic. *Public Opinion Quarterly* **86**, 913–931 (2022)

[32] Bengtsson, L., Lu, X., Thorson, A., Garfield, R., Schreeb, J.: Improved response

to disasters and outbreaks by tracking population movements with mobile phone network data: A post-earthquake geospatial study in Haiti. *PLoS Medicine* **8**, 1–9 (2011)

[33] Li, Q., Xu, B., Ma, Y., Chung, T.: Real-time monitoring and forecast of active population density using mobile phone data. In: Chen, W., Yin, G., Zhao, G., Han, Q., Jing, W., Sun, G., Lu, Z. (eds.) *Big Data Technology and Applications*, pp. 116–129 (2016)

[34] Lloyd, C.T., Sorichetta, A., Tatem, A.J.: High resolution global gridded data for use in population studies. *Scientific data* **4**, 1–17 (2017)

[35] Zipf, G.K.: The $p_1 p_2/d$ hypothesis: On the intercity movement of persons. *American Sociological Review* **11**, 677–686 (1946)

[36] Stouffer, S.A.: Intervening opportunities: A theory relating mobility and distance. *American Sociological Review* **5**, 845–867 (1940)

[37] Fik, T.J., Mulligan, G.F.: Spatial flows and competing central places: Towards a general theory of hierarchical interaction. *Environment and Planning A: Economy and Space* **22**, 527–549 (1990)

[38] Akwawua, S., Pooler, J.A.: The development of an intervening opportunities model with spatial dominance effects. *Journal of Geographical Systems* **3**, 69–86 (2001)

[39] Noulas, A., Scellato, S., Lambiotte, R., Pontil, M., Mascolo, C.: A tale of many cities: Universal patterns in human urban mobility. *PLoS One* **7**, 1–10 (2012)

[40] Sim, A., Yaliraki, S.N., Barahona, M., Stumpf, M.P.H.: Great cities look small. *Journal of The Royal Society Interface* **12**, 20150315 (2015)

[41] Simini, F., González, M.C., Maritan, A., Barabási, A.-L.: A universal model for mobility and migration patterns. *Nature* **484**, 96–100 (2012)

[42] Liang, X., Zhao, J., Dong, L., Xu, K.: Unraveling the origin of exponential law in intra-urban human mobility. *Scientific Reports* **3**, 2983 (2013)

[43] Yan, X.-Y., Zhao, C., Fan, Y., Di, Z., Wang, W.-X.: Universal predictability of mobility patterns in cities. *Journal of The Royal Society Interface* **11**, 20140834 (2014)

[44] Ren, Y., Ercsey-Ravasz, M., Wang, P., González, M.C., Toroczkai, Z.: Predicting commuter flows in spatial networks using a radiation model based on temporal ranges. *Nature Communications* **5**, 5347 (2014)

[45] Kang, C., Liu, Y., Guo, D., Qin, K.: A generalized radiation model for human mobility: Spatial scale, searching direction and trip constraint. *PLoS One* **10**,

- [46] Varga, L., Tóth, G., Néda, Z.: Commuting patterns: the flow and jump model and supporting data. *EPJ Data Science* **7**, 37 (2018)
- [47] Liu, E., Yan, X.: New parameter-free mobility model: Opportunity priority selection model. *Physica A: Statistical Mechanics and its Applications* **526**, 121023 (2019)
- [48] Liu, E.-J., Yan, X.-Y.: A universal opportunity model for human mobility. *Scientific Reports* **10**, 4657 (2020)
- [49] Du, Y., Fujiwara, N.: A modified radiation model for human mobility: Effects of distinct job-seeker expectation and job-offer benefit distributions. *IEICE Proceedings Series* **71**, 71–404 (2022)
- [50] Pappalardo, L., Simini, F., Rinzivillo, S., Pedreschi, D., Giannotti, F., Barabási, A.-L.: Returners and explorers dichotomy in human mobility. *Nature Communications* **6**, 8166 (2015)
- [51] Schläpfer, M., Dong, L., O’Keeffe, K., Santi, P., Szell, M., Salat, H., Anklesaria, S., Vazifeh, M., Ratti, C., West, G.B.: The universal visitation law of human mobility. *Nature* **593**, 522–527 (2021)
- [52] Barbosa, H., Lima-Neto, F.B., Evsukoff, A., Menezes, R.: The effect of recency to human mobility. *EPJ Data Science* **4**, 21 (2015)
- [53] Alessandretti, L., Sapiezynski, P., Sekara, V., Lehmann, S., Baronchelli, A.: Evidence for a conserved quantity in human mobility. *Nature Human Behaviour* **2**, 485–491 (2018)
- [54] Lv, J., Zhao, C., Zeng, A.: Bursty visitation of locations in human mobility. *Physica A: Statistical Mechanics and its Applications* **567**, 125674 (2021)
- [55] Aoki, T., Fujishima, S., Fujiwara, N.: Urban spatial structures from human flow by Hodge–Kodaira decomposition. *Scientific Reports* **12**, 11258 (2022)
- [56] Aoki, T., Fujishima, S., Fujiwara, N.: Identifying sinks and sources of human flows: A new approach to characterizing urban structures. *Environment and Planning B: Urban Analytics and City Science* **51**, 419–437 (2024)
- [57] Mazzoli, M., Molas, A., Bassolas, A., Lenormand, M., Colet, P., Ramasco, J.J.: Field theory for recurrent mobility. *Nature Communications* **10**, 3895 (2019)
- [58] Shida, Y., Ozaki, J., Takayasu, H., Takayasu, M.: Potential fields and fluctuation-dissipation relations derived from human flow in urban areas modeled by a network of electric circuits. *Scientific Reports* **12**, 9918 (2022)

[59] Yang, H., Lv, S., Guo, B., Dai, J., Wang, P.: Uncovering spatiotemporal human mobility patterns in urban agglomerations: A mobility field based approach. *Physica A: Statistical Mechanics and its Applications* **637**, 129571 (2024)

[60] Kodaira, K.: Harmonic fields in riemannian manifolds (generalized potential theory). *Annals of Mathematics* **50**, 587–665 (1949)

[61] Hodge, W.V.D.: *The Theory and Applications of Harmonic Integrals*. Cambridge mathematical library (Cambridge University Press), Cambridge (1989)

[62] Jiang, X., Lim, L.-H., Yao, Y., Ye, Y.: Statistical ranking and combinatorial hodge theory. *Mathematical Programming* **127**, 203–244 (2011)

[63] Benassai-Dalmau, R., Borge-Holthoefer, J., Solé-Ribalta, A.: Exploring pedestrian permeability in urban sidewalk networks. *Chaos, Solitons & Fractals* **194**, 116114 (2025)

[64] Sun, J.B., Yuan, J., Wang, Y., Si, H.B., Shan, X.M.: Exploring space–time structure of human mobility in urban space. *Physica A: Statistical Mechanics and its Applications* **390**, 929–942 (2011)

[65] Csáji, B.C., Browet, A., Traag, V.A., Delvenne, J.-C., Huens, E., Van Dooren, P., Smoreda, Z., Blondel, V.D.: Exploring the mobility of mobile phone users. *Physica A: Statistical Mechanics and its Applications* **392**, 1459–1473 (2013)

[66] Sun, H., Chen, Y., Lai, J., Wang, Y., Liu, X.: Identifying tourists and locals by k-means clustering method from mobile phone signaling data. *Journal of Transportation Engineering, Part A: Systems* **147**, 04021070 (2021)

[67] Lee, Ji-Hye, Goh, Segun, Lee, Keumsook, Choi, M. Y.: Spatiotemporal distributions of population in Seoul: joint influence of ridership and accessibility of the subway system. *EPJ Data Science*, 41 (2021)

[68] LocationMind Inc. Accessed 20 November 2024. <https://locationmind.com/>

[69] Standard grid square and grid square code used for the statistics. Accessed 20 November 2024. <https://www.stat.go.jp/english/data/mesh/02.html>

[70] Tsuboi, K., Fujiwara, N., Itoh, R.: Influence of trip distance and population density on intra-city mobility patterns in tokyo during covid-19 pandemic. *PLOS ONE* **17**, 1–22 (2022)

[71] Kato, H., Takizawa, A.: Human mobility and infection from covid-19 in the osaka metropolitan area. *npj Urban Sustainability* **2**, 20 (2022)

[72] LocationMind contact form. Accessed 20 November 2024. <https://locationmind.com/#contact-us>